Available online at www.sciencedirect.com

ScienceDirect

Physics Procedia 4 (2010) 67–83

Physics Procedia

www.elsevier.com/locate/procedia

Molecular-level understanding of environmental interfaces using density functional theory modeling

Sara E. Mason*, Christopher R. Iceman†, Thomas P. Trainor†, and Anne M. Chaka*

*Physics Laboratory, National Institute of Standards and Technology, Gaithersburg, MD, 20899.

†Department of Chemistry and Biochemistry, University of Alaska Fairbanks, Fairbanks, AK 99775

Abstract

The ability to apply existing density functional theory-based modeling techniques to timely research problems in environmental chemistry is demonstrated by an *ab initio* thermodynamics investigation of stable hydrated oxide surface models and a comparative reactivity study of Pb(II) adsorption on two water-mineral interfaces with a common geometry, but distinct electronic structure. We emphasize the unique considerations required to produce chemically reasonable structural models for hydrated surfaces and surface complex structures, as well as how to use experimental insights to limit the extensive configuration space encountered in complex hydrated models relative to theoretical surface science done under idealized, ultra-high vacuum conditions.

Keywords: Density functional theory, Surface structure, Iron oxide, Aluminum oxide, Morphology, Reactivity

1. Introduction

Hydrated oxide surfaces play key roles in modern technologies such as automotive pollution control [1], solid oxide fuel cells [2], and nanoscale biosensors [3] as well as both fundamental and applied environmental chemistry/geochemistry [4, 5, 6] and even the origins of life [7]. Surfaces under ultra-high vacuum (UHV) conditions do not exist in interfacial systems that are altered by interactions with their natural or operational environments. [5, 8] Therefore, insights from UHV surface science cannot be directly applied to understanding the solid-water interface structure and reactivity ubiquitous to earth and industrial processes. As such, a great deal of effort has been expended to characterizing metal oxide surface and particle interface structures in the past decade (e.g. [9, 10, 11, 12, 13, 14, 15, 16]). Still, a persistent barrier that remains to solving a wide range of environmental and technological problems is the current lack of molecular-level understanding about reactions at solid-water interfaces.

doi:10.1016/j.phpro.2010.08.010

Theory and modeling based on the underlying physical nature of a system offer the ability to control and compare different reactive systems. By separately varying factors such as surface composition or surface structure, the role of each factor in determining reactivity can be elucidated. Additional complexity can be added (or removed) systematically to build a framework for understanding which physical properties exert control on reactivity as well as how these factors compete or cooperate in solid-water interfaces.

First principles modeling, mainly using density functional theory (DFT) [17, 18] and *ab initio* thermodynamic analysis [19], are the primary tools used in the research summarized here. DFT calculations yield structural, force, and total energy information, as well as the system charge density. These properties enable comparison and connection with experiment and identification of underlying mechanisms through analysis of the electronic structure. In *ab initio* thermodynamics, the self-consistent total energy is used to provide an estimate of the enthalpy which may be linked to equilibria at finite temperatures and pressures to provide the Gibbs free energy of the system in contact with water [20, 19, 21, 22]. To analyze the relative Gibbs free energy of structures with varying stoichiometry, the dependence of the free energy on the chemical potentials of the components described by the material and in the environment must be considered. The surface is considered to be in chemical and thermal equilibrium with the bulk and the environment, leading to the constraint that that the chemical potentials of each type of atom must be equal in all phases. This approach allows direct theoretical determination of the influence of environment on surface structure and energetics while providing optimized geometric atomic coordinates for various surface models, ready for direct comparison with experimental results. The Gibbs free energy, defined as $G{=}H-TS$, where H is the enthalpy and S is the entropy, is the governing thermodynamic state function under conditions of fixed temperature T and pressure p. The equilibrium between the substrate and a gas phase is constrained at conditions of constant T and p such that the chemical potential of a given chemical component (μ_i) is equivalent in all phases present in the system. The surface free energy $\gamma(T, p)$, is defined as:

$$\gamma(T, p, N_i) = \frac{1}{2A}\{G_{\text{slab}}(T, p, N_i) - \sum_i N_i\mu_i(T, p)\}, \tag{1}$$

where G_{slab} is the calculated Gibbs free energy of the solid slab, N_i is the number of the ith type of atom, and A is the surface area. The factor of $(2A^{-1})$ normalizes $\gamma(T, p, N_i)$ to energy per unit area for a semi-infinite slab with two equivalent surfaces.

Here, we consider models for the α-$Al_2O_3(1\bar{1}02)$ surface with varying stoichiometry, in equilibrium with a bulk α-Al_2O_3 region, and a third region of gas-phase oxygen and water. In expressing the surface free energy of the α-$Al_2O_3(1\bar{1}02)$ surfaces, we impose that all of the species in each of the three regions are in equilibrium with each other, which allows us to relate their chemical potentials. Specifically, $2\mu_{\text{Al}}{+}3\mu_{\text{O}}{=}G^{\text{bulk}}_{\text{Al}_2\text{O}_3}$, $\mu_{\text{H}_2\text{O}}{=}G_{\text{H}_2\text{O}}{=}2\mu_{\text{H}}{+}\mu_{\text{O}}$, and $\mu_{\text{O}}{=}\frac{1}{2}G^{\text{gas}}_{\text{O}_2}{=}\frac{1}{2}\mu_{\text{O}_2}$. Therefore we have:

$$\begin{aligned} N_{\text{Al}}\mu_{\text{Al}} &= \frac{1}{2}N_{\text{Al}}G^{\text{bulk}}_{\text{Al}_2\text{O}_3} - \frac{3}{2}N_{\text{Al}}\mu_{\text{O}} \\ N_{\text{H}}\mu_{\text{H}} &= \frac{1}{2}N_{\text{H}}\mu_{\text{H}_2\text{O}} - \frac{1}{2}N_{\text{H}}\mu_{\text{O}} \end{aligned} \tag{2}$$

and,

$$\gamma(T, p, N_i) = \frac{1}{2A}\left[E_{\text{slab,0 K}} + \Delta G^{\text{vib}} - \frac{1}{2}N_{\text{Al}}\mu_{\text{Al}_2\text{O}_3} + (\frac{3}{2}N_{\text{Al}} - N_{\text{O}})\mu_{\text{O}} - N_{\text{H}}\mu_{\text{H}}\right]. \quad (3)$$

The only independent variables in our *ab initio* thermodynamic analysis are μ_{O} in equilibrium with bulk Al_2O_3, and μ_{H}. The chemical potentials of the remaining species considered in the relevant equilibria (Al, O_2, H_2, and H_2O) are dependent. In practice, meaningful application of the above outlined method requires careful consideration of theoretical errors and physical limits, as discussed in Reference [23].

We are interested in both hydrated surface morphology and reactivity. For the latter, we chose a probe adsorbate of environmental importance and for which experimental data is available. This both constrains the modeling and presents the opportunity to provide molecular-level understanding to empirically known reactivity trends. Lead (Pb) contamination is ranked as one of the most serious environmental issues by the Environmental Protection Agency and the U.S. Department of Health and Human Services' Agency for Toxic Substances and Disease Registry, with significant consequences for human health and bioaccumulation in ecosystems [24]. Within soils and sediments Pb(II) generally partitions strongly to the solid phase, both limiting dissolved concentrations in aqueous systems, and resulting in persistence of contamination in the near surface environment [25]. Among the possible modes of solid phase partitioning, adsorption of metal-ion contaminants at the aqueous interface of nanoscale metal oxide and metal (oxy)hydroxide particles is perhaps the most significant process responsible for controlling contaminant sequestration and mobility, and finds widespread use in remediation technologies [13, 26]. The reactivity of metal-(hydr)oxide phases stems from both the abundant surface area and the nature of the surface functional groups exposed to aqueous solution; generally consisting of hydroxyl moeities that can act as ligands for direct complexation of Lewis acids, Lewis base exchange sites, or sites for physical adsorption through Coulomb and hydrogen bonding (H-bonding) interactions [27, 26].

Studies of Pb binding on α-Fe_2O_3 (hematite) (0001) and $(1\bar{1}02)$ surfaces indicate that Pb(II) forms dominantly inner-sphere complexes on both surfaces, with the (0001) surface having a higher coverage of Pb(II) than the $(1\bar{1}02)$ surface based on XPS results [28]. These studies also indicate that the Fe_2O_3 surfaces are more reactive than the isostructural α-Al_2O_3 (alumina) analogs. The partitioning behavior of Pb(II) to Al_2O_3 and Fe_2O_3 single crystal substrates has been investigated further in several long-period x-ray standing wave studies of Pb(II) partitioning [29, 30, 31]. The summary of these experimental studies indicates that the Pb(II) reactivity sequence follows: α-$Fe_2O_3(0001) > \alpha$-$Al_2O_3(1\bar{1}02) \approx \alpha$-$Fe_2O_3(1\bar{1}02) >> \alpha$-$Al_2O_3(0001)$ [5]. This reactivity trend is presumably associated with the differences in surface structures of these substrates, resulting in differences in Pb(II) binding modes, as well as the intrinsic reactivity differences due to the difference in composition and electronic properties of the materials [32, 30, 5, 29, 30, 33, 28].

The complex nature of environmental interfaces mandates a thoughtful and layered approach to modeling. In our approach, a prerequisite step to studying reactivity is to first employ *ab initio* thermodynamics to solve for the lowest-energy hydrated surface structures under relevant conditions. Subsequently, reactivity is studied, here focusing on the adsorption of the Pb(II) cation. Finally, delineation of structure-property relationships is achieved by systematic comparison of adsorption energies, bonding geometries, and electronic structure analysis. In this Proceeding, we review an example from our body of work using *ab initio* thermodynamics to study and characterize an aluminum oxide surface in contact with a water and oxygen atmosphere [23]. We then summarize a comparative reactivity study aimed at addressing, for a given surface structure,

how do the differences in composition, and hence electronic structure of the substrates, influence differences in affinity for Pb(II) [34].

2. Methodology and computational details

Both the theoretical characterization of the α-$Al_2O_3(1\bar{1}02)$ surface [23] and the comparative study of Pb(II) adsorption on isostructural hydrated alumina and hematite [34] employ periodic density functional theory (DFT) calculations are carried out with the Perdew, Burke, and Ernzerhof (PBE) generalized gradient approximation (GGA) to the exchange-correlation functional [35]. All-electron calculations are performed using a double-numeric-plus-polarization, atom-centered basis set as implemented in the DMol^3 code [36, 37]. [1] Bulk lattice optimizations are converged with respect to k-points using a (5×5×5) Monkhorst-Pack grid [38] to sample the Brillouin zone, and a 4.5 Å real space cutoff (r_{cut}. In surface calculations, r_{cut} is reduced to 3.5 Å, which has been previously reported to only minimally affected resulting calculated surface free energies on hematite [39, 40]. We further test the reduction in r_{cut} on the alumina surface by considering the range of r_{cut} from 3.5 Å to 5.0 Å in 0.5 Å increments. The resulting calculated surface free energies (as defined below) vary by less than 5 meV/Å^2, within reason for the desired accuracy in the *ab initio* thermodynamic model [41]. The optimized lattice constants of 4.823 Å(+1.3%) and 13.111 Å (+0.9%) for α-Al_2O_3 and 5.044 Å (+0.1%) and 13.896Å (+0.9%) for α-Fe_2O_3 are in excellent agreement with experiment (differences from experiment are indicated in parentheses) [42, 43], and other GGA results [44, 45, 20, 46, 47, 40, 48, 39, 49]. Further details, including benchmarking, details of the employed periodic (super)cells, and a full description of the *ab initio* thermodynamics method, can be found in References [34] and [23].

Applying electronic structure methods to environmental molecular science is an exciting and new area of research. Using DFT, we are able to probe details of Pb(II) bonding interactions at a molecular level. A useful means of analyzing surface electronic structure is in terms of the density of states (DOS), a measure of the distribution of electronic energy levels in the system. The DOS can be used comparatively for different surfaces to determine the relative number of states available for adsorbate interactions above and below the surface's highest occupied energy level (or Fermi energy, E_F). In order to represent the surface electronic structure in a chemically intuitive manner, atom-projected density of states (PDOS) analysis is employed. This semi-quantitative method deconstructs the charge density into components from each atom, and for each atom, determines the s, p, and d character of the DOS. Hybridization leading to covalent interactions can be identified and traced to specific states of specific atoms through PDOS analysis [50]. In the spin-polarized hematite surfaces, the DFT eigenvalues differ between the two spin states, resulting in two PDOS data sets for each atom. As the DFT spin axis is arbitrary, the PDOS for opposite sign spins are labeled as majority and minority based on relative occupations. Here, we present PDOS plots for the Pb(II)/Al_2O_3 and Pb(II)/Fe_2O_3 systems updated relative to those presented in Reference [34]: To better characterize cation/surface bonding, we exploit a PDOS decomposition by both the l and m quantum numbers of each atomic orbital. The utility of such an "orbital-specific" PDOS analysis has been demonstrated in other adsorption systems [51], and will also be employed in our forthcoming efforts extending our comparative studies of Pb(II) on hydrated oxide surfaces.

[1] Certain commercial software is identified in this paper to foster understanding. Such identification does not imply recommendation or endorsement by the National Institute of Standards and Technology, nor does it imply that the software identified is necessarily the best available for the purpose.

(a) (b)

Figure 1: (Color Online) Model of the stoichiometric bulk termination of Al_2O_3 $(1\bar{1}02)$. Oxygen atoms are shown in red, Al atoms are in magenta. (a) Top-view showing the surface net. The first layer O, second layer Al, and third layer O are shown in a ball-and-stick representation, while the layer 4-7 Al and O atoms are shown in a line representation. The (1×1) unit cell is indicated by the dashed rectangle. The real-space vector directions are indicated. (b) Side view showing the layer stacking sequence and the full inversion-related slab model employed.

3. Density functional theory study of clean and hydrated alumina $(1\bar{1}02)$ surfaces

Reactive metal oxide surfaces are capable of dissociating water when immersed in aqueous solution, resulting in hydroxylated surfaces [5]. Understanding changes in surface morphology in going from UHV or "clean" conditions to ambient or operative conditions is therefore critical to the goal of delineating structure-reactivity relationships at the water-oxide interface. In the case of the α-$Al_2O_3(1\bar{1}02)$ surface plane, two different structures have been proposed to exist under hydrating or hydrous conditions [52, 53].

One surface scattering study concluded that the dominant termination has lost a layer of 5-fold coordinated Al atoms relative to the stoichimetric surface [52]. This "missing-Al" or "Al-vacancy" model is expected to be charge-balanced by replacing each lost Al^{3+} with 3 H^+ that form surface OH groups with lattice oxygen. An alternative surface model, also hydroxylated but with a stoichiometric termination. was posed by Catalano *et al.*, also based on surface scattering experiments [53].

Differences in surface preparation and the conditions under which measurements were made offer a hypothesis for why two sets of experiments yielded different structural results, as has been previously reported in the hematite analog [54]. Our goal in this study was to employ first principles modeling to interrogate and interpret the relative thermodynamic stabilities of different possible stoichiometries and protonation states (that is, not just the number of H-atoms on the surface, but comparison of bare oxygen, hydroxyl (-OH), and aquo ($-OH_2$) groups) of the α-$Al_2O_3(1\bar{1}02)$ surface. The study extends beyond previous theoretical work [55, 56, 57] through inclusion of more numerous and more chemically diverse surface models, including a hydrated charge-neutral model with tetrahedral surface Al atoms, as well as a set of oxygen vacancy defect surfaces discussed in the full study [23].

Surface models are generated based on the experimentally reported structures, by considering the possible ways to terminate the α-$Al_2O_3(1\bar{1}02)$ surface plane, and by exploring how to

Table 1: Surface models for the clean and hydrated α-$Al_2O_3(1\bar{1}02)$. The atoms in boldface denote layers added above the top layer of the stoichiometric termination, and X is used to indicate zero occupancy for an atomic layer that would be present in bulk layering. The repeating bulk sequence (O_2-Al_2-O_2-Al_2-O_2) is abbreviated as R

	Layer sequencing for modeled terminations						
Model	i	1	2	3	4	5	
$A1$		O_2	Al_2	O_2	Al_2	O_2	R
$A2$	$\mathbf{O_2}$	O_2	Al_2	O_2	Al_2	O_2	R
$A3$	$\mathbf{(HO)_2}$	O_2	Al_2	O_2	Al_2	O_2	R
$B1$		X	X	O_2	Al_2	O_2	R
$B2$		X	X	$(OH)_2$	Al_2	O_2	R
$C1$		O_2	X	O_2	Al_2	O_2	R
$C2$		$(HO)_2$	X	$(HO)_2$	Al_2	O_2	R
$C3$		$(HO)_2$	X	$(HO)_2$	Al_2	$(HO)_2$	R
$C4$		$(H_2O)_2$	X	$(HO)_2$	Al_2	O_2	R

achieve charge-neutrality for each stoichiometry by adding hydrogen to form -OH and -OH_2 surface groups, both with lattice oxygen or additional oxygen adatoms. The stoichiometric $(1\bar{1}02)$ geometry is depicted in top and side views in Figures 1(a) and 1(b). Using a (1×1) cell, and assuming that all oxygen atoms with common Al-coordination exist in the same protonation state, we arrive at 9 models for clean and hydrated α-$Al_2O_3(1\bar{1}02)$. Each model stoichiometry is listed in Table 1, with further structural details such as the optimized surface layer spacings, are reported in Reference [23]. We abbreviate the repeating bulk sequence (O_2-Al_2-O_2-Al_2-O_2) as R, and use boldface to indicate atomic layers of adatoms.

Prior to considering the effects of finite temperature and pressure, we first calculate the 0 K thermodynamic stabilities of the surface models across the full range of accessible μ_O. The computed values of γ(0 K) offer a baseline for understanding what surface terminations are stable under both oxygen-rich and oxygen-poor extremes, and are plotted in Figure 3(a). Also included in for comparison in Figure 3(a) is the γ(0 K) value for the clean Al-terminated α-Al_2O_3(0001) surface.[2] In agreement with chemical intuition, the minimum free energy surfaces across the range of μ_O are stoichiometric (such as A1, and Al-terminated (0001)) or sufficiently protonated to saturate surface oxygen (as in $A3$, $B2$, $C3$, $C4$). The calculated stability of these surfaces persists over a range of temperature and pressure conditions. The $A1$ stoichiometry is depicted in a side view in Figure 1(b). Side views of the optimized structures for models $A3$, $B2$, $C3$, $C4$ are shown in Figures 2(a), 2(b), 2(c), and 2(d), respectively.

To address the effects of a realistic gas-phase oxygen and water environment on predicted surface stability, we also calculate $\gamma(T)$ under both modeled UHV conditions ($p_{O_2} = p_{H_2O} = 10^{-10}$ bar) and "wet" conditions, with p_{O_2} to an ambient 20 kPa and the corresponding saturated H_2O vapor pressure at 298.15 K is 3.2 kPa. Here, we summarize the former. For the later, we discuss and present the results in Figure 3(b).

By tracing the surface(s) with the minimum value of $\gamma(T)$ under modeled UHV conditions, we arrive at 4 temperature ranges over which distinct surface terminations are stable: From 0

[2] Details of the α-Al_2O_3(0001) calculations are reported in Reference [34].

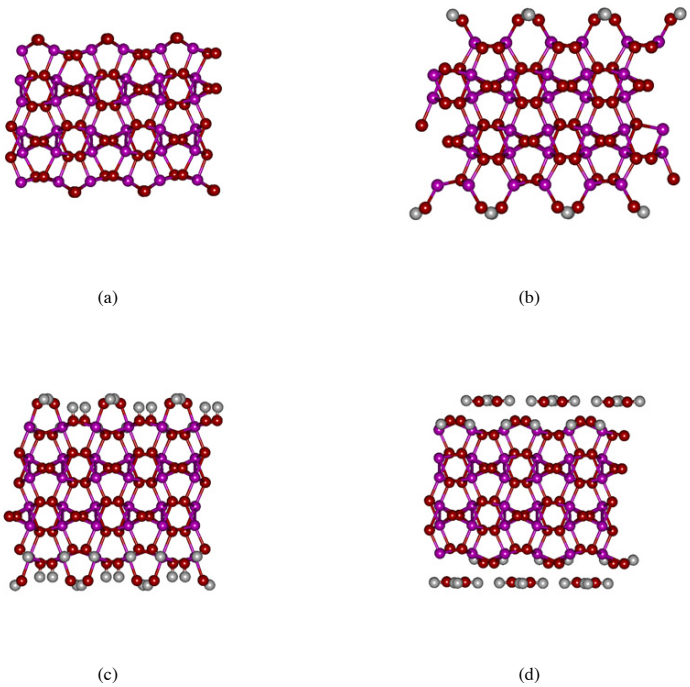

Figure 2: Side views for the minimum-energy α-Al_2O_3 $(1\bar{1}02)$ surfaces. Three repeats of the (1×1) unit cell in the y-direction are shown. Oxygen atoms are shown in red, Al atoms are in magenta. Hydrogen atoms, when present, are in gray. (a) The *A*3 model, **(HO)**$_2$-O_2-Al_2-O_2-Al_2-O_2-*R*. (b) The *B*2 model, *X*-*X*-$(OH)_2$-Al_2-O_2-*R*. (c) The *C*3 model, $(HO)_2$-*X*-$(HO)_2$-Al_2-$(HO)_2$-*R*. (d) The *C*4 model, $(H_2O)_2$-*X*-$(HO)_2$-Al_2-O_2-*R*.

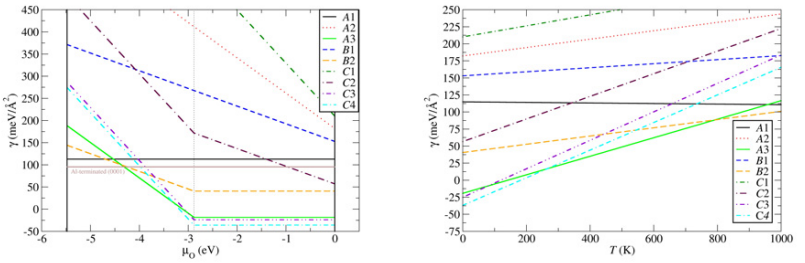

(a) (b)

Figure 3: Free energies of various surface termination models for α-$Al_2O_3(1\bar{1}02)$, and the Al-terminated (0001) surface, as determined by *ab initio* thermodynamics. Surface stoichiometries are discussed in the text and listed in Table 1. (b) Free energies of various surface termination models for α-$Al_2O_3(1\bar{1}02)$ as determined by *ab initio* thermodynamics, p_{O_2} = 20 kPa and p_{H_2O}=3.2 kPa at all temperatures. Surface stoichiometries are discussed in the text and listed in Table 1.

to 142 K, the $C4$ model has the minimum value of γ. From 142 to 451 K, the $A3$ model is preferred. Between 451 K and 593 K, the $B2$ surface is the predicted thermodynamically stable model. Finally, at T >593 K, the clean stoichiometric model $A1$ becomes preferred. In addition to the minimum energy crossings, we also predict that 5 surfaces cross the energy of the $A1$ model at different temperatures: $B2/A1$ at 593 K, $A3/A1$ at 519 K, $C4/A1$ at 396 K, $C3/A1$ at 358 K, and $C2/A1$ at 163 K.

Our interpretation of the many surface models predicted to be stable in different temperature ranges, and the numerous crossovers in γ above the minimum value surface at a given temperature, is that thermodynamically driven phases transitions between a hydrated "missing-Al" model and hydrated stoichiometric model could occur either by following the minimum surface free energy path, or by starting from a metastable configuration. The $A3/C4$ crossover at T=142 K occurs by tracing along the minimum $\gamma(T)$. Other crossovers, such as that between $B2/A1$ at 593 K, are plausible if the kinetic barrier (not included in our model) to arrive at $B2$ could be overcome under the conditions of surface preparation or measurements.

When we increase p_{O_2} and p_{H_2O} to ambient conditions, the resulting values of $\gamma(T)$ again show that several (stoichiometric or charge-neutral through hydration) surface models compete for the minimum value, as can be seen in Figure 3(b). For simplicity, we highlight on the comparison of the most preferred "missing-Al" model ($C4$) and the most preferred stoichiometric model ($A3$) under the modeled ambient conditions. At room temperate (298.15 K), the $C4$ model is preferred by just 1.8 meV/Å^2 relative to the A3 model, a difference that is smaller than the estimated 10 meV/Å^2 accuracy of the *ab initio* thermodynamic model [19].

Our interpretation of the results of γ(T) under the modeled UHV and ambient conditions is that both surface preparation and measurement conditions can influence the thermodynamically preferred surface stoichiometry. This is supported by the numerous crossovers in lower surface free energy between the stoichiometric and charge-neutral through hydration surface models.

Notably, under our modeled *in situ* conditions with p_{O_2} to an ambient 20 kPa and the corresponding saturated H_2O vapor pressure at 298.15 K is 3.2 kPa, we predict that a hydrated missing-Al structure (*C*4) is preferred up to 265 K, at which point a hydrated stoichiometric structure (*A*3) becomes the minimum energy surface. This result is helpful in interpreting the experimental observations of "missing-Al" (analogous to our *C*-series models) and hydrated sctoiciometric (analogous to our *A*3 model) surface structures.

A final consideration for the predicted thermodynamically preferred surface structures for hydrated α-$Al_2O_3(1\bar{1}02)$ is predicted implication for surface reactivity. We find two surface models with identical stoichiometries but distinct proton arrangements (*C*3, with hydroxyl groups and *C*4, with hydroxyl and aquo groups) to be within approximately 20 meV/Å^2 over a range of conditions. Though identical in stoichiometry and similar in energy, the presence of surface-bound aquo groups and intra-surface hydrogen bonding in *C*4 suggests that this surface will exhibit unique reactivity relative to other stable hydrated surface models *A*3 and *C*3. For example, using bond valence considerations [58] and the empirical model of Hiemstra *et al*. [59] to calculate pK_a values, the aquo groups are predicted to have a highly labile proton. Our studies of Pb(II) on (0001) alumina, further detailed below, demonstrate a strong role of surface hydroxyl group orientation on reactivity [34]. In forthcoming work, we present comparative studies to address how the presence of both intra-surface hydrogen bonding and aquo groups lead to distinct adsorption behavior on the *C*4 surface model.

4. Pb(II) Adsorption on Isostructural Hydrated Alumina and Hematite (0001) Surfaces

In this section, we summarize our detailed *ab initio* theoretical investigation aimed at understanding the fundamental structure-reactivity relationship of Pb(II) adsorption in a model mineral-water interface system. Full details of the study are reported in Reference [34]. Here, we emphasize considerations made in generating appropriate initial bonding geometries for the charged species on the hydrated surfaces and how we use electronic structure analysis both interpret the results and relate findings back to experimental studies.

This study focuses on Pb(II) adsorbed to the hydroxylated (0001) surface termination of α-Al_2O_3 and α-Fe_2O_3, and follows on numerous experimental investigations of Pb(II) adsorption onto iron and aluminum oxides and oxy(hydroxides) [60, 61, 62, 63, 64]. Alumina and hematite are the focus substrates of this study because of their high natural abundance and their large reactive surface areas in soil and sediment systems [65, 66, 67, 68]. Macroscopic studies of the partitioning of Pb(II) onto high-surface-area powders of iron and aluminum oxides have revealed a significant difference in the reactivity of these substrates, where in general uptake is stronger on the iron-bearing phases [68, 69, 70, 71, 72, 73]. Pb L-edge x-ray absorption spectroscopy (XAS) studies of powder systems have revealed that Pb(II) tends to bind in an inner-sphere manner (with surface functional groups satisfying the Pb(II) coordination) based on observed Pb-O and Pb-Fe(Al) distances [74, 75, 25, 76]. The body of experimental work guides and constrains our contraction of Pb(II) surface complex structures on the alumina and hematite surfaces.

The bulk corundum structure common to alumina and hematite has three unique cleavage planes to terminate the bulk to form a clean (0001) surface: a single metal ion (Fe *or* Al, labeled "M") layer, a double metal ion layer, or an oxygen layer, as indicated in the following notation: M-O_3-M-*R*, M-M-O_3-*R*, and O_3-M-M-*R*, where *R* represents the continuing bulk atomic stacking sequence.

The hydrated surface structures have been well-studied and detailed in the literature. On hematite, exposure of the stoichiometric (0001) surface to increasing partial pressure of water

vapor yields a fully hydroxylated surface [77] consistent with a $(HO)_x$-Fe-O_3-Fe-*R* structure that may persist at high p_{H_2O} [78, 79, 80, 81]. However, an analogous termination is not observed on alumina, and this stark contrast in surface structure is cited as a possible explanation for the strong affinity of Pb(II) to hematite relative to alumina. [39] The hydrated structure of the α-Al_2O_3 (0001) surface, as determined by experimental [82, 10] and theoretical [9, 20, 83] evidence, suggest a $(HO)_3$-Al-Al-*R* termination. An analogous hematite phase has been observed and in fact is predicted to be the dominant structure [39]. Therefore, the $(HO)_3$-M-M-*R* (0001) surface termination is common to both α-Fe_2O_3 and α-Al_2O_3 under realistic conditions for the mineral-water interface. This common structural phase present in distinct substrates, only one of which has *d*-electrons, offers an ideal opportunity to isolate and probe the relationship between composition and reactivity.

Periodic (1×1) cells of (0001) $(HO)_3$-M-M-*R* surfaces are too small to model Pb(II) sorption on alumina within the reported realistic concentration ranges of (0.5 to 5.2) μmol/m^2 [76], and result in concentrations high in the reported range of (2.0 to 9.92) μmol/m^2 on hematite [74]. In order to model Pb(II) sorption in a realistic coverage regime, we replicate the (1×1) surface cells into (2×2) supercells, on which one Pb atom/surface leads to coverages of (2.06 and 1.89) μmol/m^2 on alumina and hematite, respectively.

The impact of surface hydroxyl group orientation on hydrated surface reactivity has not been investigated previous to this work. Under periodic conditions, H-bond patterns form ordered surface H-bond networks. From several starting structures, we arrive at two minima. We find that the lowest energy H-bond network for both the Al_2O_3 and Fe_2O_3 surfaces is the previously reported structure for Al_2O_3, with 1 out of 3 OH groups spanning the M5 site, as shown in Figure 4. We refer to this surface H-bonded structure as "1D2U," for "one (H^+) down, two (H^+) up." A second H-bond network (not previously reported), which is essentially equivalent in energy (0.04 eV and 0.03 eV higher in energy for alumina and hematite, respectively) was also observed. We refer to this second arrangement as "2D1U," for "two (H^+) down, one (H^+) up." While the 1D2U and 2D1U structures are energetically similar, the 2D1U structure is qualitatively unique in that 2 out of every 3 OH groups span the M5 site. In the global minimum 1D2U, one OH group forms two hydrogen bonds to surface O atoms, while in the 2D1U structure, two OH groups form hydrogen bonds to the same surface O atom.

The active sites at oxide surfaces are unsaturated anions, so the binding sites are defined by the surface oxygens. We combine the result that X-ray experiments showing that Pb(II) surface complexes prefer trigonal pyramidal coordination [76] with the inherent structure of the $(HO)_3$-M-M-*R* surface, which terminates in a triangular sublattice of oxygen atoms, to identify well-defined and chemically-distinct adsorption sites for Pb(II). Specifically, the centers of these oxygen triangles inherently provide a reasonable coordination environment for Pb(II).

We generate initial starting geometries for adsorbed Pb at surface sites centered about 3 surface hydroxyl groups, with Pb about 1.5 Å above the topmost surface O-plane, (corresponding to Pb-O bond lengths of about 2.1 Å based upon experimentally observed distances) [76, 74]. We rely on alphanumeric labeling of the surface atomic layers to name the adsorption sites in terms of the initial high symmetry locations: The M2 site is defined by a triangle of layer 1 O atoms centered above a M2 cation, the metal ion closest to the topmost oxygen layer. M3 is the site above the lower cation in the metal double layer. The O4 site is centered above a non-terminal oxygen layer atom. The M5 site, which is above the metal cation in the fifth atomic layer, corresponds to the bulk continuation site on the surface. The chemically distinct (in how they relate to surface oxygen layers and the metal bilayers) sites are shown schematically in Figure 4. To achieve charge-neutrality, and in line with experimental and bond valence predictions of oxygen

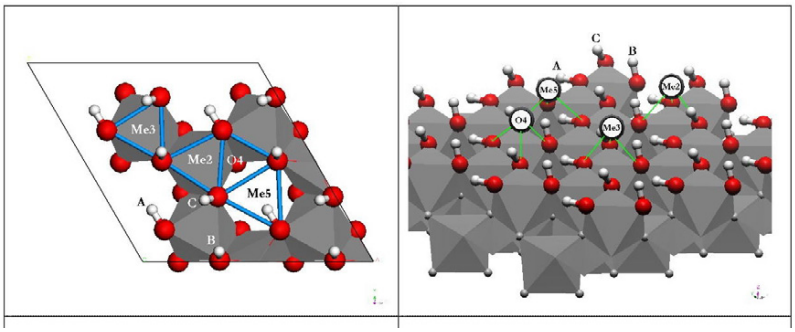

Figure 4: The fully hydroxylated oxygen terminated (0001) α-M_2O_3 surfaces. The initial Pb adsorption sites, M2, M3, O4, and M5 are indicated. H and O atoms are shown in white and red, respectively. MO_6 octahedra are indicated by gray polygons, which are centered by cations ("Me") or oxygen atoms (O). (a) Top view of the surface with the "one down two up" (1D2U) H-bond arrangement. The boundary of the (2×2) supercell is traced in black. Oxygen functional groups involved at each adsorption site are connected by green lines. The A, B, and C H^+ are labeled. (b) Perspective view of the surface with the 1D2U H-bond arrangement. Initial Pb positions for each site are indicated, with bonds to surface oxygens shown in green. The A, B, and C H^+ are indicated.

protonation states in Pb(II) surface complexes, we remove 2 of the 3 hydrogen atoms at each adsorption site. The nonequivalence of the 3 hydrogen atoms gives rise to 3 unique ways to replace two H^+ with one Pb(II) at each site (labeled as A, B, and C in Table 2, quickly multiplying the number of starting geometries considered. Note that while E_{ads} is reported for all sites and deprotonation schemes on Al_2O_3, only a subset of Pb(II) surface complex structures are optimized on Fe_2O_3. This was done intentionally, using the (computationally faster) Al_2O_3 analogs to screen potential minimum energy sorbed lead structures.

After optimization of the initial Pb(II) surface complex structures, we analyze the results in terms of energy, geometry, and electronic structure. Full details of the results are reported in Reference [34]. Here, we focus on the use of electronic structure analysis to interpret the Pb(II)/interface interactions.

In order to make comparisons between the adsorption on the two different oxide surfaces, we define the Pb adsorption energy, E_{ads}:

$$E_{ads} = \frac{1}{2}\left[(E_{surf} + 2E_{Pb(OH)_2}) - (E_{surf/Pb} + 4E_{H_2O})\right], \tag{4}$$

where E_{surf} and $E_{surf/Pb}$ are the total energies of the hydrated surface and the hydrated surface with two H^+ displaced by Pb, respectively, E_{H_2O} is the total energy of an isolated water molecule, and $E_{Pb(OH)_2}$ is the total energy of the isolated gas-phase Pb complex. Division by 2 accounts for the two equivalent surfaces. Under this sign convention, positive values represent favorable adsorption. Our choice of a gas-phase reference for Pb ($Pb(OH)_2$) is motivated by the desire to ensure that our employed methodology is capable of achieving similar accuracy in the description of all components considered. It is not a solution-phase reference, as $Pb(OH)_2$ is hypothesized to be an important atmospheric species formed from Pb emissions [84, 85]. Hydration properties of the aqueous Pb(II) cation have been studied using hybrid DFT methods [86], and in the

Table 2: Values of E_{ads}, in eV, for Pb/α-M_2O_3(0001). The adsorption site naming scheme is described in the text.

	A	B	C	A	B	C
Al_2O_3						
	1D2U			2D1U		
Al2	-0.18	-0.38	-0.77	-0.02	-0.55	-0.19
Al3	0.23	-0.02	-0.25	0.28	0.23	0.02
O4	0.07	-0.01	-0.77	-0.47	-0.99	0.10
Al5	0.07	0.12	0.12	0.06	0.13	0.36
Fe_2O_3						
	1D2U			2D1U		
Fe2	1.21			1.56		
Fe3	0.86			0.89		
Fe5			0.76			1.03

future (but beyond the scope of the present study) it may be possible to connect surface complex reactivity to such studies. Therefore, the reported relative values of E_{ads} are useful in comparing surface reactivity, the magnitudes are not representative of the energy of surface complex formation relative to the solvated Pb(II) cation.

The results for E_{ads} are presented in Table 2, and are surprising in two main ways: Despite our isolation of the common structural phase, the strongest E_{ads} of hematite is more than four times greater than that of alumina. Also, while the Al5 site is preferred on alumina, Pb(II) on hematite prefers the M2 site. The first result is outside of the hypothesis that the remarkable reactivity of α-Fe_2O_3(0001) toward Pb(II) is due to structural phases other than the $(HO)_3$-M-M-*R* surface considered here. The second result, that Pb(II) has a different site preference on the two substrates, is also unexpected. The M5 site is where the next M cation (Al or Fe) would go in the bulk registry, and is therefore the chemically intuitive ideal adsorption site. Not only is the hematite-preferred M2 site not the bulk continuation site, but it is also the site with the shortest possible distance between Pb(II) and the underlying surface cation. The calculated preference of Pb(II) at the M2 site on hematite suggests an attractive interaction is countering the inherent cation-cation repulsion present at that site.

Our explanations for the markedly high values of E_{ads} for hematite relative to alumina, and for the counter-intuitive preference Pb(II) shows for the M2 site on hematite, are both formed by PDOS analysis and interpretation.

First, we present the PDOS of Pb and O in Pb(II)/Al_2O_3. We found that Al does not participate beyond its inherent role in ionizing with oxygen in the oxide surface. The results are presented in Figure 5(a). The PDOS results show limited overlap between adsorbing Pb(II) and surface O. Significant intensity is found in both the Pb *s* and O *p* states nearly at the Fermi level, which we interpret as arising from the non-bonding Pb(II) lone pair. The only covalent interaction noted between Pb and O is at a PDOS peak only about 0.7 eV below the Fermi level.

In comparison, the PDOS of Pb(II)/Fe_2O_3 indicates stronger bonding with the surface, and also reveals a second mechanism for cation/surface interaction. The PDOS of Pb(II)/Fe_2O_3 are shown in Figure 5(b). Here, we focus on the Pb and Fe states, as we already determined the covalent interaction between Pb and O atoms by studying the PDOS of Pb and O in Pb(II)/Al_2O_3. The PDOS analysis in the hematite surface complexes reveals two ways in which the partially occupied hematite *d*-band contributes to the stability of Pb(II) adsorption. The first way is high-

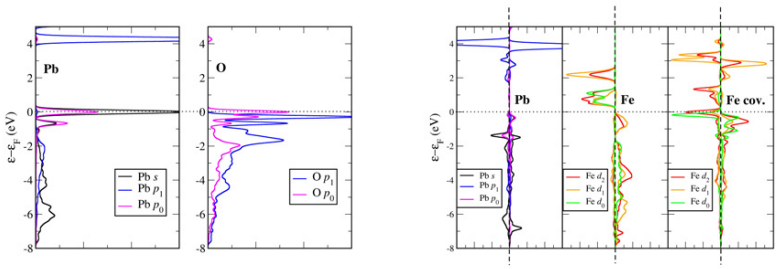

(a) (b)

Figure 5: PDOS for Pb(II)/M_2O_3. The PDOS intensity, in arbitrary units, is along the x-axis, and all plots show the same range of maximum absolute value of the PDOS. The Fermi level, ϵ_F, is set to zero and emphasized with a horizontal dotted line in both panels. (a) Pb(II)/Al_2O_3. The Pb PDOS is shown in the left panel, with the s projection shown in black. The sum of the lead $p_{m=-1,1}$ states is shown in blue and labeled as p_1. The lead $p_{m=0}$ or p_z state is shown in pink and labeled as p_0. The PDOS of an oxygen atom bonding with the adsorbed lead is shown in the right panel. The sum of the oxygen $p_{m=-1,1}$ states is shown in blue and labeled as p_1. The oxygen $p_{m=0}$ or p_z state is shown in pink and labeled as p_0. (b) Pb(II)/Fe_2O_3. The majority and minority spin values, distinguished by opposite values on the x-axis and separated by vertical dashed lines, are shown. The Pb PDOS is shown in the left panel, with the s projection shown in black. The sum of the lead $p_{m=-1,1}$ states is shown in blue and labeled as p_1. The lead $p_{m=0}$ or p_z state is shown in pink and labeled as p_0. The Fe PDOS of a typical surface Fe atom is shown in the middle panel. The sum of the iron $d_{m=-2,2}$ states is shown in red and labeled as d_2. The sum of the iron $d_{m=-1,1}$ states is shown in orange and labeled as d_1. The the iron $d_{m=0}$, or d_z^2 state, is shown in green and labeled as d_0. The right panel is the same as the middle panel, but for an Fe atom participating in a covalent Pb-O-Fe bond at the M2 site on hematite, as discussed in the text.

lighted in the middle panel in Figure 5(b), which shows a typical surface Fe *d*-band in hematite. The highest energy occupied states in the Pb(II)/Fe_2O_3 are no longer arising from Pb states as was seen in the analogous plots for alumina, but instead from the Fe *d*-band. Therefore, the same Pb-O covalent interaction observed within 0.7 eV of the Fermi level on alumina is also present on hematite, but is relatively stabilized and spans the range of 1 eV to 1.5 eV below the Fermi level. The second role of the hematite *d*-band is only observed when Pb(II) occupies the M2 sites, the same sites we find to be unexpectedly preferred. The *d*-band of the Fe atom nearest to adsorbed Pb(II) is shown in the right hand panel of Figure 5(b). Compared to the typical hematite *d*-band shown in the middle panel, the M2 Fe *d*-band is notably renormalized upon the Pb(II) adsorption. In the typical hematite Fe *d*-band, the majority(minority) spins are mostly occupied(unoccupied), showing PDOS intensity below(above) the Fermi level. While in the M2 Fe *d*-band, the majority and minority states are roughly equally populated. This is confirmed by the calculated Mulliken spins, which show that the net spin in the typical Fe is 3.66 μ_B, reduced to about 0.9 μ_B in the M2 Fe. Furthermore, there is PDOS intensity in the energy range of the Pb-O covalent interaction, suggesting metal-metal covalent bonding at this site. Therefore, the partially filled *d*-band is why Pb(II) adsorption is stronger on hematite relative to alumina, and the unexpected metal-metal interaction found at the M2 site gives rise to additional stabilization at that Pb(II) geometry. Our use of electronic structure analysis to track, explain, and interpret cation surface complexes at the water-oxide interface demonstrates an exciting opportunity to extend this type of comparative DFT-based study to other reactivity problems at environmental interfaces.

5. Concluding Remarks & Acknowledgments

In this Proceeding, we summarize work presented showing an *ab initio* thermodynamics analysis of hydrated oxide surface structure (fully reported in Reference [23]) and the results of a DFT study using electronic structure to elucidate reactivity trends in surface complexation at hydrated surfaces (fully reported in Reference [34]. These two projects demonstrate our layered approach to the theoretical study of environmental interfaces, beginning with careful surface characterization followed by thoughtfully desisted comparative studies aimed at addressing reactivity, and always using experimental information to guide and constrain the modeling.

The long-term potential and impact of first principles-based modeling of environmental interfaces lies in the theme of understanding and using the processes through which naturally adsorbing substrates react with target species. By continuing this work, we hope to build the molecular-level understanding of water-mineral interfaces, eventually casting our results into phenomenological models with predictive capabilities. Many extensions are possible, including more explicit investigations of solvation effects.

This work was supported by NSF Grants CBWT-0404400 and CHE-0431425, and utilized the high-performance computational capabilities of the Arctic Region Supercomputing Center at the University of Alaska Fairbanks, and the Helix Systems Biowulf cluster at the National Institutes of Health, Bethesda, MD. S.E.M. was supported by a National Research Council (NRC) Postdoctoral Fellowship.

References

[1] X. Xie, Y. Li, Z.-Q. Liu, M. Haruta, W. Shen, Low-temperature oxidation of CO catalyzed by Co_3O_4 nanorods, Nature 458 (2009) 746–9.

[2] R. Gorte, J. Vohs, Nanostructured anodes for solid oxide fuel cells, Current Opinion in Colloid and Interface Science 14 (2009) 236–44.
[3] A. V. Whitney, J. W. Elam, S. L. Zou, A. V. Zinovev, P. C. Stair, G. C. Schatz, R. P. Van Duyne, Localized surface plasmon resonance nanosensor: A high-resolution distance-dependence study using atomic layer deposition, J. Phys. Chem. B 109 (2005) 20522–28.
[4] G. Waychunas, C. S. Kim, J. F. Banfield, Nanoparticulate iron oxide minerals in soils and sediments: unique properties and contaminant scavenging mechanisms, J. of Nanoparticle Research 7 (2005) 409–33.
[5] G. E. Brown, Jr., T. P. Trainor, A. M. Chaka, Geochemistry of mineral surfaces and factors affecting their chemical reactivity, in: A. Nilsson, L. Pettersson, J. Nørskov (Eds.), Chemical bonding at surfaces and interfaces, Elsevier, Amsterdam, 2007, pp. 547–509.
[6] V. H. Grassian, Surface science of complex environmental interfaces: Oxide and carbonate surfaces in dynamic equilibrium with water vapor, Surf. Sci. 602 (2008) 2955–62.
[7] R. M. Hazen, Life's rocky start, Scientific American 284 (2001) 76–85.
[8] N. P. Padture, M. Gell, E. H. Jordan, Thermal barrier coatings for gas-turbine engine applications, Science 296 (2002) 280–84.
[9] K. C. Hass, W. F. Schneider, A. Curioni, W. Andreoni, The chemistry of water on alumina surfaces: Reaction dynamics from fist principles, Science 282 (1998) 265–8.
[10] P. J. Eng, T. P. Trainor, G. E. Brown, Jr., G. A. Waychunas, M. Newville, S. R. Sutton, M. L. Rivers, Structure of the hydrated α-Al_2O_3 (0001) surface, Science 288 (2000) 1029–33.
[11] F. M. Michel, L. Ehm, S. M. Antao, P. L. Lee, P. J. Chupas, G. Liu, D. R. Strongin, M. A. A. Schoonen, B. L. Phillips, J. B. Parise, The structure of ferrihydrite, a nanocrystalline material, J. Am. Chem. Soc. 316 (2007) 1726–1729.
[12] S. V. Yanina, K. M. Rosso, Linked reactivity at mineral-water interfaces through bulk crystal conduction, Science 320 (2008) 218–22.
[13] M. F. Hochella, Jr., S. K. Lower, P. A. Maurice, R. L. Penn, N. Sahai, D. L. Sparks, B. S. Twining, Nanominerals, mineral nanoparticles, and earth systems, Science 319 (2008) 1631–35.
[14] A. Navrotshy, L. Mazeina, J. Majzlan, Size-driven structural and thermodynamic complexity in iron oxides, Science 319 (2008) 1635–38.
[15] J. D. Kubicki, G. P. Halada, P. Jha, B. L. Phillips, Quantum mechanical calculation of aqueous uranium complexes: carbonate, phosphate, organic and biomolecular species, Chemistry Central Journal 3 (2009) 10–1–29.
[16] P. J. Feibelman, The first wetting layer on a solid, Phys.Today 63 (2010) 34–39.
[17] P. Hohenberg, W. Kohn, Inhomogeneous electron gas, Phys. Rev. 136 (1964) B864–71.
[18] W. Kohn, L. J. Sham, Self-consistent equations including exchange and correlation effects, Phys. Rev. 140 (1965) A1133–8.
[19] K. Reuter, M. Scheffler, Composition, structure, and stability of RuO_2(110) as a function of oxygen pressure, Phys. Rev. B 65 (2001) 035406–1–11.
[20] X.-G. Wang, A. Chaka, M. Scheffler, Effect of the environment on α-Al_2O_3(0001) surface structures, Phys. Rev. Lett. 84 (2000) 3650–3.
[21] K. Reuter, M. Scheffler, Composition and structure of the RuO_2(110) surface in an O_2 and CO environment: Implications for the catalytic formation of CO_2, Phys. Rev. B 68 (2003) 045407–1–11.
[22] Q. Sun, K. Reuter, M. Scheffler, Effect of a humid environment on the surface structure of RuO_2(110), Phys. Rev. B 67 (2003) 205424–1–7.
[23] S. E. Mason, C. R. Iceman, T. P. Trainor, A. M. Chaka, Density functional theory study of clean, hydrated, and defective alumina ($1\bar{1}02$) surfaces, Phys. Rev. B 81 (2010) 125423–1–16.
[24] http://www.atsdr.cdc.gov.
[25] J. Ostergren, G. Brown, Jr., G. Parks, T. Tingle, Quantitative speciation of lead in selected mine tailings from Leadville, CO, Environmental Science & Technology 33 (1999) 1627–36.
[26] D. Sparks, Toxic metals in the environment: The role of surfaces, Elements 1 (2005) 193–7.
[27] T. Hiemstra, H. Yong, W. Van Riemsdijk, Interfacial charging phenomena of aluminum (hydr)oxides, Langmuir 15 (1999) 5942–55.
[28] J. R. Bargar, T. P. Trainor, J. P. Fitts, S. A. Chambers, G. E. Brown, Jr., In situ grazing-incidence extended x-ray absorption fine structure of Pb(II) chemisorption on hematite (0001) and ($1\bar{1}02$) surfaces, Langmuir 20 (2004) 1667–73.
[29] T. Trainor, A. Templeton, G. B. G. Parks, Application of the long-period X-ray standing wave technique to the analysis of surface reactivity: Pb(ii) sorption at alpha-Al2O3/aqueous solution interfaces in the presence and absence of Se(vi), Langmuir 18 (2002) 5782–91.
[30] A. S. Templeton, T. P. Trainor, S. J. Traina, A. M. Spormann, G. E. Brown, Jr., Pb(ii) distributions at biofilm-metal oxide interfaces, Proc. Natl. Acad. Sci. U. S. A. 98 (2001) 11897–902.
[31] T. H. Yoon, T. P. Trainor, P. Eng, J. R. Bargar, G. E. Brown, Jr., Trace metal ion partitioning at polymer film-metal

oxide interfaces: Long-period x-ray standing wave study, Langmuir 21 (2005) 4503–11.
[32] J. R. Bargar, S. N. Towle, G. E. Brown, Jr., G. A. Parks, XAFS and bond-valence dtermination of the structures and compositions of surface functional groups and Pb(II) and Co(II) sorption products on single-crystal α-Al_2O_3, J. Colloid and Interface Science 185 (1997) 473–92.
[33] J. R. Bargar, S. N. Towle, G. E. Brown, Jr., G. A. Parks, Outer-sphere Pb(II) adsorbed at specific surface sites on single crystal α-alumina, Geochimica et Cosmochimica Acta 61 (1996) 3541–7.
[34] S. E. Mason, C. R. Iceman, K. Tanwar, T. P. Trainor, A. M. Chaka, Pb(II) adsorption on isostructural hydrated alumina and hematite (0001) surfaces: A DFT study, J. Phys. Chem. C 113 (2009) 2159–70.
[35] J. P. Perdew, K. Burke, M. Ernzerhof, Generalized gradient approximation made simple, Phys. Rev. Lett. 77 (1996) 3865–8.
[36] B. Delley, An all-electron numerical method for solving the local density functional for polyatomic molecules, J. Chem. Phys. 92 (1990) 508–17.
[37] B. Delley, From molecules to solids with the $DMol^3$ approach, J. Chem. Phys. 18 (2000) 7756–64.
[38] H. J. Monkhorst, J. D. Pack, Special points for brillouin-zone integrations, Phys. Rev. B 13 (1976) 5188–5192.
[39] T. P. Trainor, A. M. Chaka, P. J. Eng, M. Newville, G. A. Waychunas, J. G. Catalano, G. E. Brown, Jr., Structure and reactivity of the hydrated hematite (0001) surface, Surf. Sci. 573 (2004) 204–24.
[40] C. S. Lo, K. S. Tanwar, A. M. Chaka, T. P. Trainor, Density functional theory study of the clean and hydrated hematite ($1\bar{1}02$) surfaces, Phys. Rev. B 75 (2007) 075425–1–15.
[41] K. Reuter, M. Scheffler, Composition, structure, and stability of RuO_2(110) as a function of oxygen pressure, Phys. Rev. B 65 (2002) 035406–1–11.
[42] Crystal Structures, Vol. 2, John Wiley and Sons, 1964.
[43] L. W. Finger, R. M. Hazen, Crystal-structure and isothermal compression of Fe_2O_3,Cr_2O_3, and V_2O_3 to 50 kbars, J. Appl. Phys. 51 (1980) 5362–67.
[44] R. Meyer, Q. Ge, J. Lockmeyer, R. Yeates, M. Lemanski, D. Reinalda, M. Neurock, An *ab initio* analysis of adsorption and diffusion of silver atoms on alumina surfaces, Surf. Sci. 601 (2007) 134–45.
[45] B. Hinnemann, E. A. Carter, Adsorption of Al, O, Hf, Y, Pt, and S atoms on α-Al_2O_3(0001), J. Phys. Chem. C 111 (2007) 7105–26.
[46] C. Ruberto, Y. Yourdshahyan, B. I. Lundqvist, Surface properties of metastable alumina: A comparative study of κ- and α-Al_2O_3, Phys. Rev. B 67 (2003) 195412–195430.
[47] X. G. Wang, W. Weiss, S. K. Shaikhutdinov, M. Ritter, M. Petersen, F. Wagner, R. Schlogl, M. Scheffler, The hematite (α-Fe_2O_3) (0001) surface: Evidence for domains of distinct chemistry, Phys. Rev. Lett. 81 (1998) 1038–41.
[48] S. E. Mason, E. A. Sokol, V. R. Cooper, A. M. Rappe, Spontaneous formation of dipolar metal nanoclusters, J. Phys. Chem. A 113 (2009) 4134–37.
[49] A. Rohrbach, J. Hafner, G. Kresse, Ab initio study of the (0001) surfaces of hematite and chromia: Influence of strong electronic correlations, Phys. Rev. B 70 (2004) 125426–1–17.
[50] R. Hoffman, A chemical and theoretical way to look at bonding on surfaces, Rev. Mod. Phys. 60 (1988) 601–28.
[51] S. E. Mason, I. Grinberg, A. M. Rappe, Orbital-specific analysis of CO chemisorption on transition-metal surfaces, J. Phys. Chem. C 112 (2008) 1963–66.
[52] T. P. Trainor, P. J. Eng, G. E. Brown, Jr., I. K. Robinson, M. D. Santis, Crystal truncation rod diffraction study of the alpha-Al_2O_3 ($1\ \bar{1}\ 0\ 2$) surface, Surf. Sci. 496 (2002) 238–50.
[53] J. G. Catalano, C. Park, Z. Zhang, P. Fenter, Termination and water adsorption at the α-Al_2O_3(012)-aqueous solution interface, Langmuir 22 (2006) 4668–73.
[54] K. S. Tanwar, J. G. Catalano, S. C. Petitto, S. K. Ghose, P. J. Eng, T. P. Trainor, Hydrated α-Fe_2O_3($1\bar{1}02$) surface structure: Role of surface preparation, Surf. Sci. Lett. 601 (2007) L59–L64.
[55] J. Guo, D. E. Ellis, D. J. Lam, Electronic structure and energetics of sapphire (0001) and ($1\bar{1}02$) surfaces, Phys. Rev. B 45 (1992) 13647–13656.
[56] A. Marmier, S. Parker, Ab initio morphology and surface thermodynamics of α-Al_2O_3, Phys. Rev. B 69 (2004) 115409–1–4.
[57] L. G. V. Briquet, C. R. A. Catlow, A. A. French, Platinum group metal adsorption on clean and hydroxylated corundum surfaces, J. Phys. Chem. C 113 (2009) 16747–56.
[58] I. Brown, K. K. Wu, Empirical parameters for calculating cation-oxygen bond valences, Acta. Cryst. B32 (1976) 1957–9.
[59] T. Hiemstra, H. Yong, W. Van Riemsdijk, Intrinsic proton affinity of reactive surface groups of metal (hydr)oxides: The bond valence principle, J. Coll. Interf. Sci. 184 (1996) 680–92.
[60] A. Manceau, M.-C. Boisset, G. Sarret, J.-L. Hazemann, M. Mench, P. Cambier, R. Prost, Direct determination of lead speciation in contaminated soils by exafs spectroscopy, Environ. Sci. Technol. 30 (1996) 1540–52.
[61] C. E. Martínez, M. McBride, Dissolved and labile concentrations of cd, cu, pb, and zn in aged ferrihydrite-organic matter systems, Environmental Science & Technology 33 (1999) 745–50.

[62] E. J. Elzinga, D. Peak, D. L. Sparks, Spectroscopic studies of pb(ii)-sulfate interactions at the goethite-water interface, Geochimica et Cosmochemica Acta 65 (2001) 2219–30.
[63] D. Dong, Y. Nelson, L. Lion, M. Shuler, W. Ghiorse, Adsorption of pb and cd onto metal oxides and organic material in natural surface coatings as determined by selective extractions: new evidence for the importance of mn and fe oxides, Water Research 34 (2000) 427–36.
[64] M. Villalobos, M. Trotz, J. Leckie, Surface complexation modeling of carbonate effects on the adsorption of cr(vi), pb(ii), and u(vi) on goethite, Environmental Science & Technology 35 (2001) 3849–56.
[65] U. Schwertmann, Solubility and dissolution of iron-oxides, Plant and Soil 130 (1991) 1–25.
[66] S. Stipp, M. Hansen, R. Kristensen, M. Hochella, L. Bennedsen, K. Dideriksen, T. Balic-Zunic, D. Leonard, H. Mathieu, Behaviour of fe-oxides relevant to contaminant uptake in the environment, Chemical Geology 190 (2002) 321–37.
[67] G. Sposito, Surface-reactions in natural aqueous colloidal systems, Chimia 43 (1989) 169–76.
[68] W. Stumm, J. Morgan, Aquatic Chemistry, Wiley, 1996.
[69] G. E. Brown, Jr., G. Parks, Sorption of trace elements on mineral surfaces: Modern perspectives from spectroscopic studies, and comments on sorption in the marine environment, International Geology Review 43 (2001) 963–1073.
[70] G. E. Brown, Jr., N. Sturchio, An overview of synchrotron radiation applications to low temperature geochemistry and environmental science, Applications of Synchrotron Radiation in Low-Temperature Geochemistry and Environmental Sciences 49 (2002) 1–115.
[71] P. Schindler, Surface complexes at oxide water interfaces, in: M. Anderson, A. Rubin (Eds.), Adsorption of Inorganics at Solid-Liquid Interfaces, Ann Arbor Science Publishers, Inc., Ann Arbor, 1981, pp. 1–49.
[72] K. Hayes, L. Katz, Application of X-ray absorption spectroscopy for surface complexation modeling of metal ion sorption, in: P. Brady (Ed.), Physics and Chemistry of Mineral Surfaces, CRC Press, Boca Raton, 1996, pp. 147–223.
[73] D. A. Dzomback, F. Morel, Surface Complexation Modeling; Hydrous Ferric Oxide, John Wiley and Sons, New York, 1990.
[74] J. R. Bargar, G. E. Brown, Jr., G. A. Parks, Surface complexation of Pb(II) at oxide-water interfaces: II. XAFS and bond-valence determination of mononuclear and polynuclear Pb(II) sorption products on iron oxides, Geochimica et Cosmochimica Acta 61 (1997) 2639–52.
[75] J. D. Ostergren, T. P. Trainor, J. R. Bargar, G. E. Brown, Jr., G. A. Parks, Inorganic ligand effects on pb(ii) sorption to goethite (alpha-feooh) - i. carbonate, Journal of Colloid and Interface Science 225 (2000) 466–82.
[76] J. R. Bargar, G. E. Brown, Jr., G. A. Parks, Surface complexation of Pb(II) at oxide-water interfaces: I. XAFS and bond-valence determination of mononuclear and polynuclear Pb(II) sorption products on aluminum oxides, Geochimica et Cosmochimica Acta 61 (1997) 2617–37.
[77] P. Liu, T. Kendelewicz, G. E. Brown, Jr., E. J. Nelson, S. A. Chambers, Reaction of water vapor with α–Al_2O_3(0001) and α–Fe_2O_3 surfaces: Synchrotron X-ray photoemission studies and thermodynamic calculations, Surf. Sci. 417 (1998) 53–65.
[78] C. M. Eggleston, A. G. Stack, K. M. Rosso, S. R. Higgins, A. M. Bice, S. W. Boese, E. D. Pribul, J. J. Nichols, The structure of hematite (α–Fe_2O_3) (001) surfaces in aqueous media: Scanning tunneling microscopy and resonant tunnerling calculations of coexisting o and fe terminations, Geochimica et Cosmochimica Acta 67 (2003) 985–1000.
[79] U. Becker, M. Hochella, E. Apra, The electronic structure of hematite (001) surfaces: Applications to the interpretation of STM images and heterogeneous surface reactions, American Mineralogist 81 (1996) 1301–14.
[80] P. Venema, T. Hiemstra, P. Weidler, W. van Riemsdijk, Intrinsic proton affinity of reactive surface groups of metal (hydr)oxides: Application to iron (hydr)oxides, Journal of Colloid and Interface Science 198 (1998) 282–95.
[81] S. Yin, X. Ma, D. E. Ellis, Initial stages of H_2O adsorption and hydroxylation of Fe-terminated α–Fe_2O_3 surface, Surf. Sci. 601 (2007) 2426–37.
[82] S. A. Chambers, T. Droubay, D. R. Jennison, T. R. Mattsson, Laminer growth of ultrathin metal films on metal oxides: Co on hydroxylated alpha-al2o3(0001), Science 297 (2002) 827–31.
[83] K. C. Hass, W. F. Schneider, A. Curioni, W. Andreoni, First-principles molecular dynamics simulations of H_2O on α-Al_2O_3 (0001), J. Phys. Chem. B 104 (2000) 5527–40.
[84] A. T. Benjelloun, A. Daoudi, H. Chermette, Interaction of lead atom with atmospheric hydroxyl radical: An ab initio and density functional theory study of the resulting complexes PbOH and HPbO, J. Chem. Phys. 121 (2004) 7207–21.
[85] A. Benjelloun, A. Daoudi, H. Chermette, Ab initio and density functional theory study of lead complexes of atmospheric interest Pb(H-2), Pb(OH), Pb(H2O), Pb(HO2) and Pb(OH)(2), Molecular Physics 103 (2005) 317–35.
[86] M. Wander, A. Clark, Hydration properties of aqueous Pb(II) ion, Inorganic Chemistry 47 (2008) 8233–41.